*URSI - RCRS 2024, ARIES/GEHU, Bhimtal, India, 22 - 25 October, 2024*

# Land-cover Type Classification Over Sundarbans Using the Optical Bands and the Kennaugh Parameters from Sentinel Sensors

Sukanya Mukherjee(1), and Subhadip Dey(1)
(1) Agricultural and Food Engineering Department, Indian Institute of Technology Kharagpur, India

## Abstract

Analysis of the land cover types is critical for understanding land use patterns and forecasting sustainable land management as it utilizes precise, high-resolution spatio-temporal information from Synthetic Aperture Radar (SAR) and Optical data. In this study, we used the Kennaugh matrix elements derived from the dual polarimetric Sentinel-1 SAR data and the optical bands of the Sentinel-2 data for land cover classification over the Indian Sundarban region. We demonstrated the variations of the Kennaugh elements and the optical bands for Eleven land cover classes and then showed the combined utilization of these elements for improved classification of the land cover targets. The overall accuracy and Kappa coefficients for each class were used to evaluate the classification results. Significantly improved results were obtained through the joint utilization of the Kennaugh elements and the optical bands, which allowed enhanced discrimination among the land cover targets, viz., Mangroves, Built-Up Areas, and Shallow Water Areas.

## 1 Introduction

Wetlands are one of the most essential ecosystems, often found adjacent to fresh and saline water areas. They are mainly characterized by hydric soils, which may remain inundated periodically or permanently depending on the topographic variations and growth stage [1]. Despite the vast extent of wetlands and their advantages, inventory mapping is limited and irregular. However, with the advent of remote sensing data, the land cover classification over the wetland area has gained significant interest [2, 3]. Van et al. [4] utilized the high-resolution RapidEye data to separate nine wetland and dryland communities over four seasons. It was found that the classification accuracy is reduced during the autumn and winter seasons. In another study, Ávila et al. [5] revealed the deterioration of the water storage capacity of Bajo Sinú Wetlands Complex in Columbia using optical and thermal bands of Landsat-7 and Landsat-8.

The overall accuracies for the previous pixel-level classification technique ranged around $\approx$ 70-84 %. Hence, Frohn et al. [6] proposed a segmentation and object-based classification technique which outperformed the overall classification accuracies obtained from the traditional algorithms. However, accurate large-scale wetland mapping with sole optical remote sensing data remains challenging due to atmospheric and target-related noises.

In this aspect, due to its long wavelength, the Synthetic Aperture Radar (SAR) data gets less impacted by the atmospheric constituents. Moreover, the SAR data gives an overview of the target bio-physical parameter, while the optical data provides information on the target bio-chemical parameters. Also, poor fens are almost non-separable from bogs, while a high mixture of information exists between the peatland and upland forest. Moreover, the extent of water in wetlands is often underestimated using optical data [7]. Therefore, SAR data, in addition to the optical data, increases the information space about a target. Besides, due to the long wavelength of the SAR signal, it can penetrate the subsurface level. Hence, it can provide subcanopy-level information about the vegetation in wetland areas [8].

In this regard, using optical data from Landsat-7 and the HH polarization of Radarsat-1 SAR sensor improved the separability of wetland features to some extent [9]. However, there is still a need for clarification between the peatland, upland forest, and bog-fen. Hence, Touzi et al. [10, 11] used the L-band PALSAR data, which showed enhanced separation between the open bogs and poor fens. Besides, Betbeder et al. [12] studied the sensitivity of the Shannon entropy with wetland flooding status and vegetation roughness using the X-band TerraSAR-X data. In a similar line, Mahdianpari et al. [13] utilized ALOS-2 L-band, RADARSAT-2 C-band, and TerraSAR-X data to classify wetland classes in the Avalon Peninsula hierarchically. Similarly, several optical and SAR data classify some land-cover types over the Sundarban region [14, 15, 16].

Although several studies classified wetlands using SAR data, most of the studies are limited to only backscatter intensity values. Some studies utilized the SAR signature-based analysis and optimization technique, which was computationally expensive and increased confusion among some land-cover types for dual polarimetric cases. On the other hand, the Kennaugh elements derived from SAR data are essential for the scattering target monitoring [17, 18]. However, the variations of these elements concerning wetland classes are not adequately detailed in the literature. The Kennaugh representation characterizes both coherent and incoherent targets. Thus, in this study, we utilized the

Kennaugh matrix elements derived from the dual polarimetric Sentinel-1 SAR data and the optical bands from the Sentinel-2 sensor to classify the land-cover types over the Sundarban area, India.

## 2 Study area and Datasets

The extent of Indian Sundarban Region ($20°31'$ to $22°30'$ N, and $88°10'$ to $89°51'$ E) stretches to the southwestern part of the Ganga and Brahmaputra rivers with a total area of 423 000 ha (Figure 1). The study location includes two districts of West Bengal, i.e., North and South 24 Parganas. Sundarban is well known for its largest mangrove vegetation, which can be broadly classified into fresh and saline-water loving categories. The study area receives the highest rainfall event during the monsoon, while the humidity generally varies from 80 % to 94 %. As the area contains marine deposits, various shoals, ridges, and flats can be found. We have used Sentinel-1 and Sentinel-2 data of month April 2023 to identify eleven different land cover classes over the study site, which are: Agriculture (AG), Fallow Land (FL), Built- up Area (BA), Marshy Land (ML), Shallow Water Area (SWA), Mangrove (M), Tidal Mud Flat (TMF), Sandbar (S), Estuary (E), Vegetation (V) and Periodically Inundated Land (PIL) respectively.

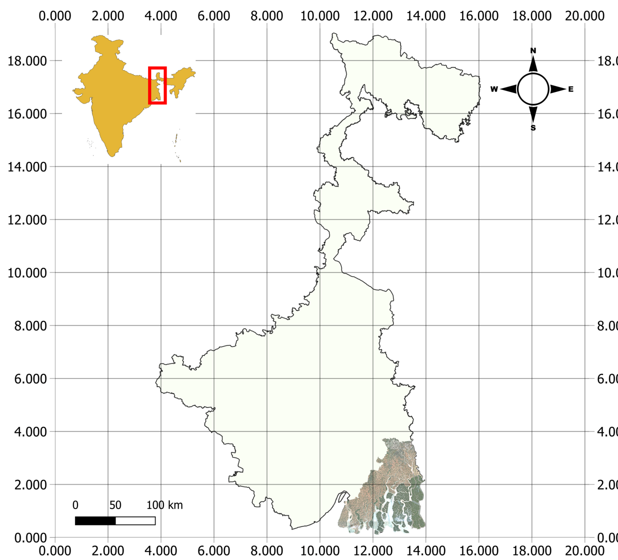


**Figure 1.** The study area over the Sundarbans wetland. The true color RGB is composed using the Sentinel-2 data, acquired during April, 2023.

## 3 Methodology

For full polarimetric SAR measurement, the scattering matrix (**S**) encompasses the complete information about the scattering characteristics of a target. **S** can be represented as,

$$\mathbf{S} = \begin{bmatrix} S_{XX} & S_{XY} \\ S_{YX} & S_{YY} \end{bmatrix} \tag{1}$$

where $X$ and $Y$ are either horizontal ($H$) and vertical ($V$) polarization channels and $XY$ denotes $X$ as transmit and $Y$ as received polarizations, respectively. However, the complex notation of the elements of **S** may not be able to provide an in-depth insight about the target. Hence, another suitable representation in terms of the power is given by the $4 \times 4$ real Kennaugh matrix (**K**) [17]. The transfomration from the complex scattering matrix to the real Kennaugh matrix can be given as,

$$\mathbf{K} = \frac{1}{2}\mathbf{A}^*(\mathbf{S} \otimes \mathbf{S}^*)\mathbf{A}^H, \quad \mathbf{A} = \begin{bmatrix} 1 & 0 & 0 & 1 \\ 1 & 0 & 0 & -1 \\ 0 & 1 & 1 & 0 \\ 0 & j & -j & 0 \end{bmatrix}, \tag{2}$$

For monostatic SAR acquisitions, the cross-polar channels are identical, i.e., $S_{XY} = S_{YX}$, and hence, **K** becomes symmetric. However, for dual polarimetric SAR data, the $2 \times 2$ **S** matrix does not exists. Depending on the type of system, either $\begin{bmatrix} S_{XX} & S_{XY} \end{bmatrix}$ or, $\begin{bmatrix} S_{YX} & S_{YY} \end{bmatrix}$ can be obtained. As a result, some of the elements of the Kennaugh matrix vanishes and **K** becomes sparse. For a dual polarimetric case, where the transmit polarization is $Y$ and the received polarization is $X$, the Kennaugh matrix can be expressed as,

$$\mathbf{K} = \begin{bmatrix} K_0 & 0 & K_5 & 0 \\ 0 & K_1 & 0 & K_8 \\ K_5 & 0 & 0 & 0 \\ 0 & 0 & 0 & 0 \end{bmatrix} \tag{3}$$

where,

$$\begin{aligned} K_0 &= |S_{VV}|^2 + |S_{VH}|^2 \\ K_1 &= |S_{VV}|^2 - |S_{VH}|^2 \\ K_5 &= \Re(S_{VV}S_{VH}^*) \\ K_8 &= -\Im(S_{VV}S_{VH}^*) \end{aligned}$$

$\Re$ and $\Im$ are the real and imaginary part of an element, respectively. Additionally, we have utilized the optical bands, i.e., red, green, blue and near infrared from Sentinel-2 sensor. Following this, we have applied the Extreme Gradient Boosting (XGB) classifier with 600 trees to individual optical data, Kennaugh elements and optical-Kennaugh fused data.

## 4 Results and Discussion

Three scenarios were established for the classification of images in the experimental analysis, and the effects of the variables were assessed. First, in this section we have shown the accuracy scores in Table 1 along with the classified map using the fused optical and Kennaugh elements data in Figure 2. From Table 1, it can be observed that the overall accuracy of the classification was 98.71 % for Sentinel-2, while, 95.58 % for Kennaugh elements, and 99.40 % for the fused data. For each of these categories the Kappa coefficients were 0.83, 0.81, and 0.87, respectively. Moreover, we observed highest classification accuracy for M and E using the Kennaugh elements, while the additional use of the optical data increased the classification accuracy over V, ML, FL and BA classes.

**Table 1.** Precision, Recall and overall (OA) accuracy for Kennaugh elements and Sentinel-2 data over different land cover features in Sundarbans, West Bengal, India using Extreme Gradient Boosting (XGB) classifier

| | | **XGB** | | | |
|---|---|---|---|---|---|
| | | **Precision** | **Recall** | **Overall accuracy** | **$\kappa$** |
| | SWA | 56 | 29 | | |
| | AG | 64 | 64 | | |
| | FL | 62 | 36 | | |
| | BA | 30 | 5 | | |
| | ML | 41 | 31 | | |
| Kennaugh elements | M | 90 | 99 | 95.58 | 0.81 |
| | TMF | 57 | 26 | | |
| | S | 54 | 19 | | |
| | E | 98 | 100 | | |
| | V | 37 | 3 | | |
| | PIL | 18 | 3 | | |
| | SWA | 87 | 78 | | |
| | AG | 95 | 96 | | |
| | FL | 82 | 93 | | |
| | BA | 52 | 31 | | |
| | ML | 79 | 76 | | |
| Sentinel-2 bands | M | 97 | 99 | 98.71 | 0.83 |
| | TMF | 85 | 87 | | |
| | S | 95 | 85 | | |
| | E | 100 | 100 | | |
| | V | 40 | 11 | | |
| | PIL | 58 | 54 | | |
| | SWA | 97 | 95 | | |
| | AG | 97 | 98 | | |
| | FL | 95 | 95 | | |
| | BA | 75 | 54 | | |
| | ML | 96 | 92 | | |
| Kennaugh and Sentinel-2 | M | 98 | 100 | 99.40 | 0.87 |
| | TMF | 92 | 94 | | |
| | S | 96 | 90 | | |
| | E | 100 | 100 | | |
| | V | 67 | 32 | | |
| | PIL | 79 | 80 | | |

High misclassification rate of those classes using the only Kennaugh elements shown in Figure 3(a). From boxplot a high confusion can be found between AG and, FL. The median value of FL is similar to AG. In a similar way, the median value of SWA is similar to E. As a result, great extent of SWA also misclassified as E within the study area.

Although, when we observed misclassification among different land cover features, the fused bands showed better results. The overall classification accuracy was approximately $\approx 4$ %, higher than the classification accuracy of the Kennaugh elements. The increased classification accuracy might be due to the significant separations of median values of different bands for the land cover features, which can be seen in Figure 3. Although the classification accuracy was significantly improved compared to the other bands, a good amount of confusion still exists between the vegetation and built-up areas, as can be seen in Figure 2. This confusion might be because of the $K_1$ element that produced similar backscatter intensity over V, like BA, due to the underlying water surface. As a result we observe low precision and recall scores over BA, which were 75 and 54 %, respectively. Similarly, over V, the precision and recall scores dropped to 67 and 32 %, respectively.

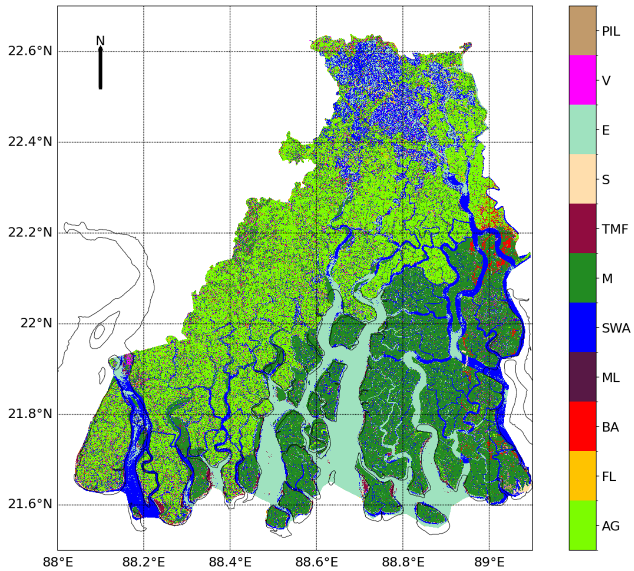


**Figure 2.** The classified map of Sundarban wetland using the Sentinel-1 and 2 data, acquired during April, 2023.

## 5 Conclusions

The study presents a classification technique based on the Kennaugh matrix elements from Sentinel-1 data and optical bands from the Sentinel-2 data. We found that the joint utilization of the Kennaugh matrix elements and the optical bands better discriminate several land-cover targets within the Indian Sundarban wetland compared to individual use of that sets. However, a large number of features might be required to improve class- wise accuracies. The research results could be used further to analyze Sentinel-1 and Sentinel-2 data with additional classes.


## 6 Acknowledgement

The authors would like to thank European Space Agency (ESA) for providing the Sentinel-1 and Sentinel-2 data. The study was funded by the GISE-hub IIT Bombay through project receipt grant No. 3/69/2021/NSDI(G)(E.No.36454)/GISE2023/0001018773-01


## References


[1] M. Mahdianpari, B. Salehi, F. Mohammadimanesh, S. Homayouni, and E. Gill, "The first wetland inventory map of newfoundland at a spatial resolution of 10 m using sentinel-1 and sentinel-2 data on the google earth engine cloud computing platform," *Remote Sensing*, vol. 11, no. 1, p. 43, 2018.

[2] A. L. Gallant, "The challenges of remote monitoring of wetlands," pp. 10 938–10 950, 2015.

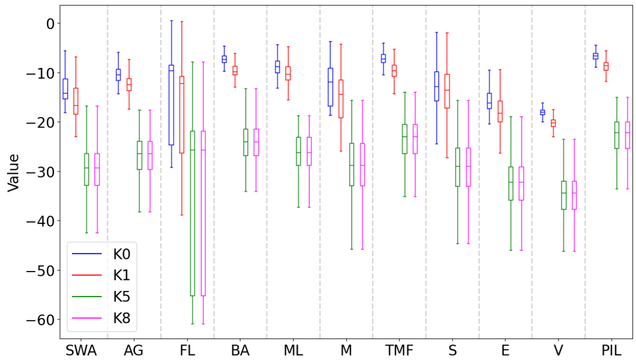


(a) Kennaugh elements

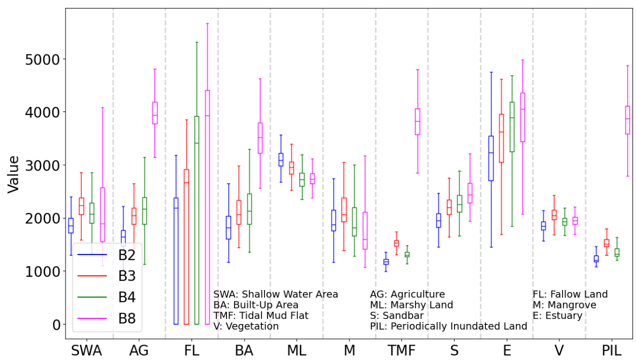


(b) Sentinel-2 data

**Figure 3.** Box plots of the Kennaugh elements and the Sentinel-2 bands over different land cover features of Sundarbans, West Bengal, India


[3] F. Mohammadimanesh, B. Salehi, M. Mahdianpari, and S. Homayouni, “Unsupervised wishart classfication of wetlands in newfoundland, canada using polsar data based on fisher linear discriminant analysis,” *The International Archives of the Photogrammetry, Remote Sensing and Spatial Information Sciences*, vol. 41, pp. 305–310, 2016.

[4] H. van Deventer, M. A. Cho, and O. Mutanga, “Multi-season rapideye imagery improves the classification of wetland and dryland communities in a subtropical coastal region,” *ISPRS Journal of Photogrammetry and Remote Sensing*, vol. 157, pp. 171–187, 2019.

[5] D. Mejia Ávila, V. C. Soto Barrera, and Z. Martínez Lara, “Spatio-temporal modelling of wetland ecosystems using landsat time series: case of the bajo sinú wetlands complex (bswc)–córdoba–colombia,” *Annals of GIS*, vol. 25, no. 3, pp. 231–245, 2019.

[6] R. Frohn, B. Autrey, C. Lane, and M. Reif, “Segmentation and object-oriented classification of wetlands in a karst florida landscape using multi-season landsat-7 etm+ imagery,” *International Journal of Remote Sensing*, vol. 32, no. 5, pp. 1471–1489, 2011.

[7] R. Touzi, K. Omari, B. Sleep, and X. Jiao, “Scattered and received wave polarization optimization for enhanced peatland classification and fire damage assessment using polarimetric palsar,” *IEEE Journal of Selected Topics in Applied Earth Observations and Remote Sensing*, vol. 11, no. 11, pp. 4452–4477, 2018.

[8] M. Salvia, M. Franco, F. Grings, P. Perna, R. Martino, H. Karszenbaum, and P. Ferrazzoli, “Estimating flow resistance of wetlands using sar images and interaction models,” *Remote Sensing*, vol. 1, no. 4, pp. 992–1008, 2009.

[9] M. Grenier, A.-M. Demers, S. Labrecque, M. Benoit, R. A. Fournier, and B. Drolet, “An object-based method to map wetland using radarsat-1 and landsat etm images: Test case on two sites in quebec, canada,” *Canadian Journal of Remote Sensing*, vol. 33, no. sup1, pp. S28–S45, 2007.

[10] R. Touzi, G. Gosselin, J. Li, and R. Brook, “Peatland subsurface water monitoring using polarimetric l-band palsar,” in *PolinSAR 2011 Proceedings*, 2011.

[11] R. Touzi, G. Gosselin, and R. Brook, “Polarimetric l-band sar for peatland mapping and monitoring,” *ESA Book on Principles and Applications of Pol-InSAR. Springer*, 2015.

[12] J. Betbeder, S. Rapinel, S. Corgne, E. Pottier, and L. Hubert-Moy, “Terrasar-x dual-pol time-series for mapping of wetland vegetation,” *ISPRS Journal of Photogrammetry and Remote Sensing*, vol. 107, pp. 90–98, 2015.

[13] M. Mahdianpari, B. Salehi, F. Mohammadimanesh, and M. Motagh, “Random forest wetland classification using alos-2 l-band, radarsat-2 c-band, and terrasar-x imagery,” *ISPRS Journal of Photogrammetry and Remote Sensing*, vol. 130, pp. 13–31, 2017.

[14] R. Dwivedi, B. Rao, and S. Bhattacharya, “Mapping wetlands of the sundaban delta and it’s environs using ers-1 sar data,” *International Journal of Remote Sensing*, vol. 20, no. 11, pp. 2235–2247, 1999.

[15] M. Rahman, R. Ullah, M. Lan, J. Sri Sumantyo, H. Kuze, and R. Tateishi, “Comparison of landsat image classification methods for detecting mangrove forests in sundarbans,” *International journal of remote sensing*, vol. 34, no. 4, pp. 1041–1056, 2013.

[16] K. Awty-Carroll, P. Bunting, A. Hardy, and G. Bell, “Using continuous change detection and classification of landsat data to investigate long-term mangrove dynamics in the sundarbans region,” *Remote Sensing*, vol. 11, no. 23, p. 2833, 2019.

[17] A. Schmitt, A. Wendleder, and S. Hinz, “The kennaugh element framework for multi-scale, multi-polarized, multi-temporal and multi-frequency sar image preparation,” *ISPRS Journal of Photogrammetry and Remote Sensing*, vol. 102, pp. 122–139, 2015.

[18] S. Dey, D. Mandal, L. D. Robertson, B. Banerjee, V. Kumar, H. McNairn, A. Bhattacharya, and Y. Rao, “In-season crop classification using elements of the kennaugh matrix derived from polarimetric radarsat-2 sar data,” *International Journal of Applied Earth Observation and Geoinformation*, vol. 88, p. 102059, 2020.